# High-spin states and the first signs of band termination in $^{156}$Ho

D. M. Cullen
*Nuclear Structure Research Laboratory, University of Rochester, 271 East River Road, Rochester, New York 14627 and Oliver Lodge Laboratory, Department of Physics, University of Liverpool, Liverpool L69 7ZE, United Kingdom*

C.-H. Yu,* D. Cline, and M. Simon
*Nuclear Structure Research Laboratory, University of Rochester, 271 East River Road, Rochester, New York 14627*

D. C. Radford*
*Chalk River National Laboratories, Atomic Energy of Canada Limited, Chalk River, Ontario, Canada K0J 1J0*

M. A. Riley
*Department of Physics, Florida State University, Tallahassee, Florida 32306*

J. Simpson
*C.C.L.R.C., Daresbury Laboratory, Daresbury, Warrington, WA4 4AD, United Kingdom*
(Received 13 November 1997)

High-spin states have been populated in $^{156}$Ho with the $^{14}$N+$^{148}$Nd reaction at 96 MeV. The known level scheme has been considerably extended using the Gammasphere spectrometer. Configuration assignments for these bands have been deduced from their aligned angular momenta, signature splittings and from a systematic survey of the neighboring nuclei and these are compared with theoretical $B(M1)/B(E2)$ predictions from a semiclassical model. Evidence is also presented for the onset of band termination, or the beginning of a prolate collective to oblate noncollective shape change near the yrast line, at the highest spin states in two of the observed strongly coupled bands. [S0556-2813(98)01905-0]

PACS number(s): 27.70.+q, 23.20.Lv, 21.10.Re

## I. INTRODUCTION

Historically odd-odd nuclei have always proven difficult to study. This is because of their high single-particle level density, at low excitation energy, which results in a multitude of near-yrast bands or configurations. As an example of these complexities, the ground-state spin of the odd-odd nucleus $^{156}$Ho has been difficult to establish and remains uncertain. To date arguments have been presented for ground-state spin assignments of $I=1\hbar$ [1] and $I=4\hbar$ [2] from hyperfine interaction measurements and $I=5\hbar$ from the electron-capture decay of $^{156}$Er, [3] and also $I=9\hbar$ [4]. However, it is precisely the fact the odd-odd nuclei have been somewhat neglected in the past which makes their study, with the new generation of powerful $\gamma$-ray spectrometers, particularly attractive.

In the mass 150 region the study of odd-odd nuclei has been mainly restricted to low spins. These odd-odd studies have played an important role in demonstrating the shape-driving effects of high-$j$ intruder orbits and that these nuclei are ''soft'' with respect to triaxial deformations [5]. In addition, odd-odd nuclei have served as useful references in assigning configurations in the neighboring nuclei.

This paper describes the results of an experiment which populated high-spin states in the odd-odd nucleus $^{156}_{67}\mathrm{Ho}_{89}$. The known level scheme has been considerably extended and evidence is presented for a change in structure, signified by the onset of band termination, at the highest spin states in two of the rotational bands. The transition to band termination is accompanied by a change in nuclear shape in the yrast states from a well-deformed prolate to a weakly-deformed oblate shape [6,7]. Such behavior might be expected for $^{156}$Ho because some of the rotational bands in the neighboring isotopes $^{155}_{67}$Ho [7] and $^{157}_{67}$Ho [8] and isotones $^{155}_{66}$Dy [9] and $^{157}_{68}$Er [10], are observed to terminate in fully aligned configurations at large angular momentum $I\approx 30-40\hbar$.

## II. EXPERIMENT

High-spin states were populated in $^{156}$Ho with the $^{148}$Nd($^{14}$N,6$n$) reaction at 96 MeV. Stacked thin ($\approx$800 $\mu$g/cm$^2$) targets of $^{148}$Nd, enriched to 94.1%, were used. Triple- and higher-fold coincidence events were collected at a rate of $\approx$3000 per second. A total of $\approx 10^9$ unfolded triple-coincident events were collected with the thirty-six escape-suppressed germanium detectors of the Gammasphere array [11] at the Lawrence Berkeley Laboratory. The 36 detectors were arranged in three rings of five at each of the forward and backward angles of 17.3°, 31.7°, and 37.4° and the remaining six detectors were in a ring at 90° with respect to the beam direction.

The data were sorted into a three-dimensional matrix or ''cube'' and a triple-coincidence analysis was performed with the LEVIT8R code [12]. Double-gates were placed in this cube and the $\gamma$-ray intensities and coincidence relationships were used to determine the order of the $\gamma$ rays in the level

*Present address: Physics Division, Oak Ridge National Laboratory, Oak Ridge, Tennessee 37831.

 

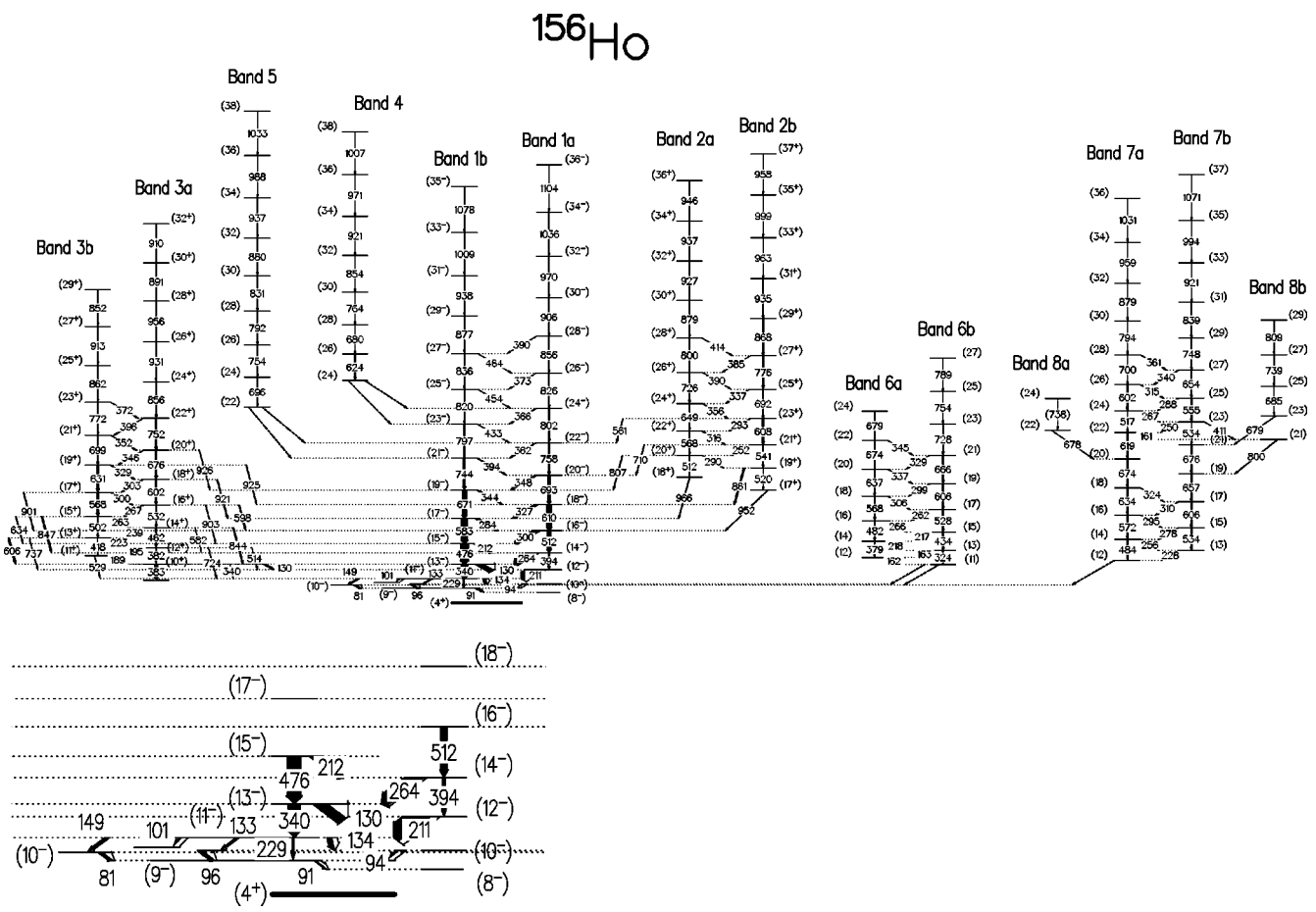


FIG. 1. (a) The level scheme for $^{156}$Ho showing the new bands (bands 2a, 3a, 4, 5, 8a, and 8b) and the extensions to the known bands (bands 1a, 1b, 2b, 3b, 6a, 6b, 7a, and 7b). Note that the ground-state spin is uncertain (see text) and in the figure all spins are drawn relative to a ground-state spin which is assumed to be $4\hbar$ at zero excitation energy. (b) A partial level scheme for $^{156}$Ho which shows the lower-spin region of bands 1a and 1b expanded for clarity.

scheme. In addition, a two-dimensional matrix was constructed in which all events in coincidence with one of the six 90 ° detectors were incremented on one of the axes. The other axis contained those events in coincidence with any other non-90 ° detector. The angular correlation ratios, $R = I(\text{for})/I(90)$ extracted from these matrices, were used to determine the multipolarity of the $\gamma$ rays using the directional correlation from orientated states (DCO) method [13].

### III. RESULTS

The new level scheme for $^{156}$Ho, extracted from these data, is shown in Figs. 1(a) and 1(b). In the present study the known [4,7,14–16] yrast rotational bands in $^{156}$Ho (bands 1a and 1b) have been extended and six new bands (bands 2a, 3b, 4, 5, 8a and 8b) have been established. The average intensity of these bands, relative to the yrast band 1b, are given in Table I. In the introduction it was pointed out that the ground-state spin of $^{156}$Ho has not been definitely established. In this paper the $I = 4\hbar$ assignment [2] will be used throughout; however, all spins and parities are uncertain and are shown in parentheses in Figs. 1(a) and 1(b). The DCO ratios for some of the most intense $\gamma$-ray transitions are given in Table II. With these data it was not always possible to obtain DCO ratios for the highest-spin transitions in any of these bands due to their small intensities. In this case those in-band $\gamma$-ray transitions were generally assumed to be $\Delta I = 2$ transitions if their energies were reasonably smooth extensions of the lower-spin collective rotational states.

The yrast band 1a has been extended [7] from spin $(24)\hbar$ to spin $(36)\hbar$ and its signature-partner band 1b has been extended from spin $(29)\hbar$ [7] to spin $(35)\hbar$; see Fig. 1(a). The DCO ratios for the transitions in bands 1a and 1b are consistent with those of other known $\Delta I = 2$ quadrupole transitions in $^{156}$Ho; see Table II. Seven new interband transitions between bands 1a and 1b were also established; see

TABLE I. The average intensities of the bands observed in $^{156}$Ho normalized to band 1b at low rotational frequencies.

| Band | % Intensity signature (0) a | % Intensity signature (+1) b |
|---|---|---|
| 1 | 51.2±1.5 | 100±1.9 |
| 2 | 8.5±0.3 | 8.5±0.4 |
| 3 | 19.0±1.1 | 21.9±1.1 |
| 4 | 4.8±0.4 | ⋯ |
| 5 | 2.8±0.3 | ⋯ |
| 6 | 11.6±0.5 | 14.5±0.6 |
| 7 | 14.5±0.7 | 14.7±0.7 |
| 8 | 6.4±0.3 | 4.1±0.3 |

TABLE II. The DCO ratios for bands 1, 2, 3, and 7 in $^{156}$Ho. The symbol <1.0 indicates that the transition was more intense in the 90° relative to the forward-spectrum. DCO ratios were not calculated for some transitions since they were too weak and/or heavily contaminated by other $\gamma$ rays with similar energies. (The weakest intensity transitions were generally only assigned in the level scheme after a series of double-gated spectra were summed.)

| $E_\gamma$ | DCO ratio (Band 1a) | Assignment | $E_\gamma$ | DCO ratio (Band 1a) | Assignment |
|---|---|---|---|---|---|
| 91 | 1.02±0.19 | $E2$ | 710 | 0.52±0.04 | Dipole ($E1$) |
| 130 | 0.57±0.05 | $\Delta I=1$, $M1/E2$ | 861 | 0.45±0.03 | Dipole ($E1$) |
| 264 | 0.60±0.04 | $\Delta I=1$, $M1/E2$ | 952 | <1.0 | Dipole |
| 300 | 0.55±0.01 | $\Delta I=1$, $M1/E2$ | $E_\gamma$ | DCO ratio (Band 3a) | Assignment |
| 327 | 0.61±0.04 | $\Delta I=1$, $M1/E2$ | 195 | 0.66±0.10 | $\Delta I=1$, $M1/E2$ |
| 394 | 0.93±0.08 | $E2$ | 239 | 0.57±0.05 | $\Delta I=1$, $M1/E2$ |
| 512 | 0.95±0.06 | $E2$ | 382/383 | 0.98±0.08 | $E2$ |
| 610 | 1.04±0.09 | $E2$ | 462 | 1.03±0.07 | $E2$ |
| 693 | 0.92±0.11 | $E2$ | 532 | 1.00±0.04 | $E2$ |
| 758 | 1.08±0.12 | $E2$ | 602 | 1.01±0.05 | $E2$ |
| 802 | 0.90±0.12 | $E2$ | 676 | 0.87±0.06 | $E2$ |
| $E_\gamma$ | DCO ratio (Band 1b) | Assignment | 752 | 0.97±0.07 | $E2$ |
| 134 | 0.67±0.03 | $\Delta I=1$, $M1/E2$ | 856 | 0.83±0.09 | $E2$ |
| 211/212 | 0.58±0.01 | $\Delta I=1$, $M1/E2$ | 931 | 0.97±0.14 | $E2$ |
| 284 | 0.59±0.06 | $\Delta I=1$, $M1/E2$ | 956 | 1.20±0.28 | $E2$ |
| 340 | 0.96±0.06 | $E2$ | 130 | 0.45±0.05 | Dipole |
| 476 | 0.98±0.01 | $E2$ | 340 | 0.59±0.06 | $\Delta I=1$ ($M1$) |
| 583 | 1.03±0.07 | $E2$ | 582 | 0.90±0.10 | $\Delta I=0$ ($M1$) |
| 671 | 1.00±0.13 | $E2$ | 844 | 0.62±0.04 | $\Delta I=1$ ($M1$) |
| 744 | 0.97±0.07 | $E2$ | 724 | 0.69±0.06 | $\Delta I=1$ ($M1$) |
| 797 | 0.98±0.19 | $E2$ | $E_\gamma$ | DCO ratio (Band 3b) | Assignment |
| 820 | 1.06±0.25 | $E2$ | 223 | 0.66±0.07 | $\Delta I=1$, $M1/E2$ |
| $E_\gamma$ | DCO ratio (Band 2a) | Assignment | 263 | 0.51±0.03 | $\Delta I=1$, $M1/E2$ |
| 290 | 0.59±0.10 | $\Delta I=1$, $M1/E2$ | 418 | 1.04±0.13 | $E2$ |
| 316 | 0.47±0.07 | $\Delta I=1$, $M1/E2$ | 502 | 0.93±0.11 | $E2$ |
| 356 | 0.48±0.17 | $\Delta I=1$, $M1/E2$ | 568 | 1.12±0.08 | $E2$ |
| 512 | 0.92±0.11 | $E2$ | 631 | 0.89±0.03 | $E2$ |
| 568 | 0.94±0.19 | $E2$ | 699 | 0.91±0.07 | $E2$ |
| 649 | 1.45±0.28 | $E2$ | 772 | 0.96±0.07 | $E2$ |
| 726 | 0.87±0.10 | $E2$ | 529 | 1.19±0.23 | $\Delta I=0$ ($E2/M1$) |
| 800 | 0.61±0.07 | $E2$ | | | |
| 879 | 1.00±0.17 | $E2$ | 606 | 0.94±0.11 | $\Delta I=0$ ($E2/M1$) |
| 927 | 1.07±0.27 | $E2$ | | | |
| 807 | 0.49±0.08 | Dipole ($E1$) | 737 | 1.15±0.10 | $M1$ |
| 966 | 0.55±0.19 | Dipole ($E1$) | 847 | 0.84±0.08 | $M1$ |
| $E_\gamma$ | DCO ratio (Band 2b) | Assignment | 901 | 0.36±0.04 | $M1$ |
| 252 | 0.54±0.07 | $\Delta I=1$, $M1/E2$ | $E_\gamma$ | DCO ratio (Band 7a) | Assignment |
| 293 | 0.52±0.08 | $\Delta I=1$, $M1/E2$ | 228 | 0.40±0.02 | $M1$ |
| 541 | 0.91±0.16 | $E2$ | 572 | 0.91±0.07 | $E2$ |
| 608 | 0.95±0.10 | $E2$ | 619 | 1.16±0.10 | $E2$ |
| 692 | 0.91±0.11 | $E2$ | $E_\gamma$ | DCO ratio (Band 7b) | Assignment |
| 776 | 0.97±0.14 | $E2$ | 606 | 1.09±0.05 | $E2$ |
| 868 | 0.87±0.12 | $E2$ | 676 | 1.21±0.09 | $E2$ |
| 935 | 1.02±0.13 | $E2$ | 800 | 1.31±0.18 | $E2$ |

Figs. 1(a) and 2(a). These transitions have DCO ratios which are consistent with those of other known $\Delta I=1$ mixed $M1/E2$ transitions in $^{156}$Ho.

Four members of band 2b were previously reported in Ref. [7]. However, in that study band 2b was proposed to directly decay into the yrast states. The present data disagree with the previous decay pattern in that band 2b is connected to the yrast band 1a by four new transitions (561, 710, 861 and 952 keV); see Fig. 1(a). Band 2b has also been extended by two transitions (999 and 958 keV) and nine members of its signature-partner rotational band, band 2a, have been established; see Fig. 2(b). Band 2a is also connected to the yrast bands 1a and 1b at spins (17) and (19) by two new transitions (at 966 and 807 keV). Nine interband transitions

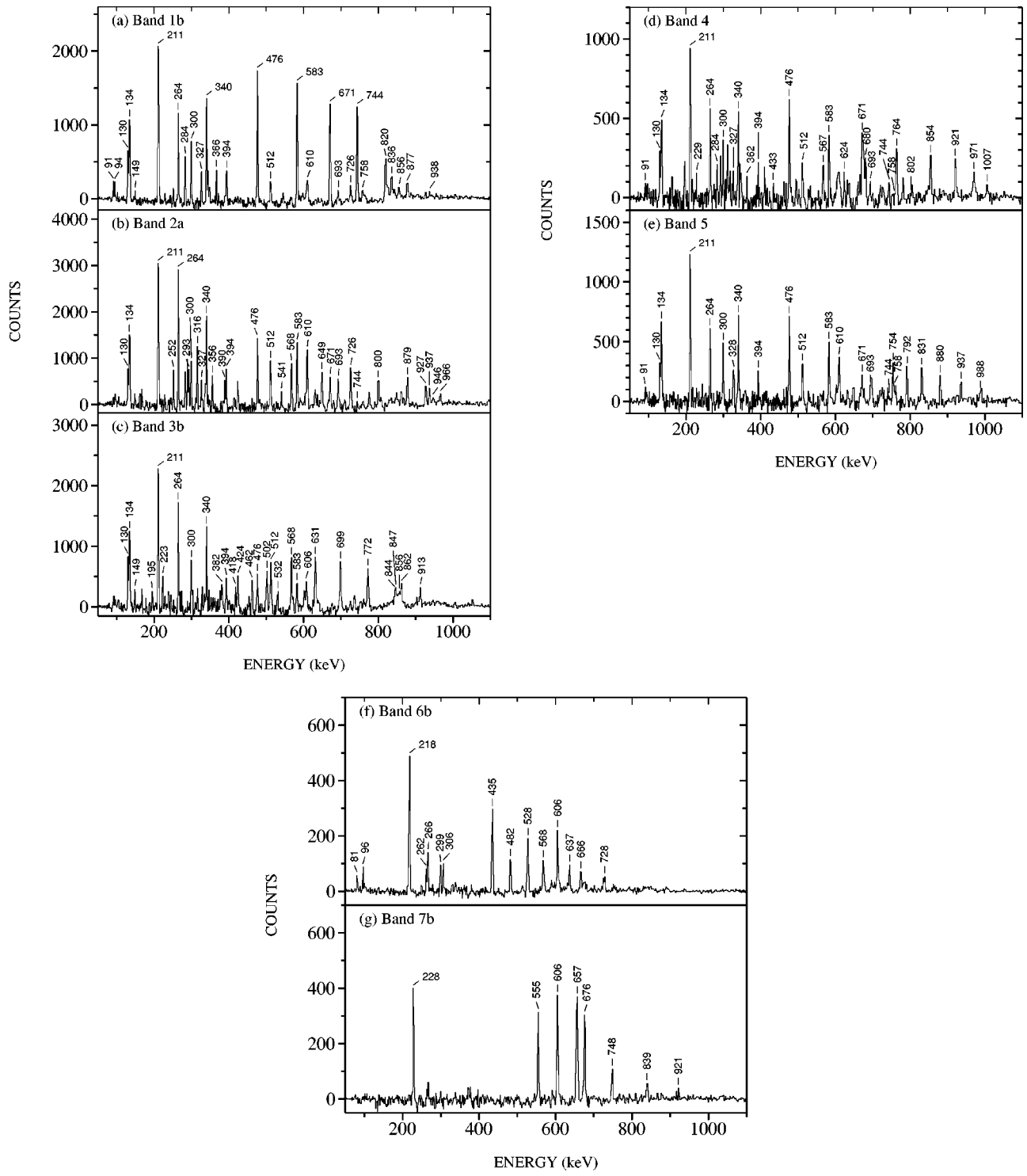


FIG. 2. (a) A sum of 6 double-gates in band 1b (the 797 keV with the 134- to 744-keV transitions). (b) A sum of 36 double-gated spectra for band 2a (the sum includes all the in-band transitions double gated with the 512-keV transition). (c) A sum of 21 double-gated spectra for band 3b from all of the combinations of the 502- to 913-keV transitions). (d) A sum of all of the doubled-gated combinations of the 624- to 1007-keV transitions in band 4. (e) A sum of all of the doubled-gated combinations of the in-band transitions in band 5. (f) A double-gated spectrum (the 162- with the 163-keV transition) on band 6b. (g) A double-gated spectrum (the 534- with the 534-keV transition) on band 7b.

were also observed to link these signature-partner bands. These interband transitions have DCO ratios which are consistent with those of other $\Delta I=1$ mixed $M1/E2$ transitions and are shown in Table II.

Five members of band 3a were also previously reported in Ref. [7] and this band has been extended by five new stretched $E2$ transitions. In addition the lowest spin $\gamma$-ray transition in band 3b (502.5 keV) was previously reported in Ref. [15]; however, the present data disagree with the two higher in-band transitions which were reported at 607.6 and 725.0 keV and also with its decay into the yrast band 1a (via a 381.9-keV transition). These two proposed in-band transitions in Ref. [15] are in fact established, in this work, as transitions which link this band into the yrast states. Band 3b

is connected to the yrast bands 1a and 1b by seven new transitions and band 3a by eleven new transitions; see Figs. 1(a) and 2(c). In addition the eight new members of band 3b are shown in Fig. 1(a). Bands 3a and 3b are linked by thirteen new interband transitions. These interband transitions have DCO ratios which are consistent with those of other $\Delta I=1$ mixed $M1/E2$ transitions; see Table II.

The newly established bands 4 and 5 display different behavior to the other rotational bands in $^{156}$Ho in that only one signature is observed; see Figs. 1(a), 2(d) and 2(e). The decoupled band 5 decays to the yrast bands 1a and 1b around spin (21) to $(22)\hbar$; see Fig. 2(e). Band 5 is observed to be in coincidence with the yrast band up to the 744- and 758-keV transitions and therefore, the lowest observed spin in band 5 must be $\geqslant (21-22)\hbar$. However, the discrete $\gamma$-ray linking transitions could not be established. The decoupled band 4 is composed of a new sequence of seven $\Delta I=2$ transitions; see Fig. 1(a). Band 4 is observed to be in coincidence with the yrast band up to the 758- and 802-keV transitions at spin $(22-24)\hbar$ and the lowest observed spin in band 4 must be $\geqslant(24)\hbar$. However, like band 5, the discrete linking transitions could not be established.

The strongly coupled bands 6a and 6b were first reported in Ref. [7]. In the present work bands 6a and 6b have been extended with one new transition in band 6a (679 keV) and two new transitions in band 6b (754 and 789 keV) and by one dipole connecting transition (345 keV). It was not possible to link this band into the yrast states because its intensity is weak and fragmented. However, the transitions in the band are observed in coincidence with the 81- and 96-keV transitions of the low-spin states; see Fig. 2(f).

Band 7b was previously established by Waddington *et al.* [14] where four states in one signature of band 7b and one in the other signature band 7a were observed. The 228.2-keV transition which was reported to link band 7b to the yrast states is in conflict with our data which show that the $(12^-)$ to $(11^-)$ 211-keV transition is not in coincidence with the 228-keV transition; see Fig. 2(g). The transitions which link bands 7a and 7b into the yrast states were not observed in these data probably due to their low intensity and/or fragmented decay path. After the third in-band transition bands 7a and 7b backbend and two new sequences have been established to high spin; see Fig. 1(a). In addition, at the same rotational frequency another two signatures, bands 8a and 8b, are observed to decay into bands 7a and 7b, respectively. The DCO ratios for some of these transitions are given in Table II.

## IV. DISCUSSION

In order to establish configurations for the newly observed rotational bands and to confirm the configurations of the existing bands in $^{156}$Ho a systematic survey of the neighboring nuclei has been performed. Cranked-shell model (CSM) and total Routhian surface (TRS) calculations, based on those described in [17], predict that the yrast configuration has a deformation which is characterized by a prolate shape ($\beta_2=0.21$, $\beta_4=0.02$, and $\gamma\approx 0^0$) at low rotational frequencies ($\hbar\omega<0.4$ MeV) which becomes slightly $\gamma$ soft at higher rotational frequencies. Table III summarizes the labeling convention used in this work for the lowest orbitals around the $N=89$ and $Z=67$ Fermi surfaces.

TABLE III. The convention for labeling the lowest orbitals around the neutron $N=89$ and the proton $Z=67$ Fermi surfaces. The integer $n$ refers to the $n$th orbit of a particular parity $\pi$ and signature $\alpha$.

| Label | Asymptotic Nilsson neutron state ($\hbar\omega=0$) | $(\pi,\alpha)_n$ |
|---|---|---|
| A | $i_{13/2}$ [660]1/2 | $(+,+1/2)_1$ |
| B | $i_{13/2}$ [660]1/2 | $(+,-1/2)_1$ |
| C | $i_{13/2}$ [651]3/2 | $(+,+1/2)_2$ |
| D | $i_{13/2}$ [651]3/2 | $(+,-1/2)_2$ |
| E | $h_{9/2}$ [521]3/2 | $(-,+1/2)_1$ |
| F | $h_{9/2}$ [521]3/2 | $(-,-1/2)_1$ |
| X | $h_{11/2}$ [505]11/2 | $(-,+1/2)_2$ |
| Y | $h_{11/2}$ [505]11/2 | $(-,-1/2)_2$ |
| Label | Asymptotic Nilsson proton state ($\hbar\omega=0$) | $(\pi,\alpha)_n$ |
| $A_p$ | $h_{11/2}$ [523]7/2 | $(-,-1/2)_1$ |
| $B_p$ | $h_{11/2}$ [523]7/2 | $(-,+1/2)_1$ |
| $E_p$ | $g_{7/2}$ [404]7/2 | $(+,-1/2)_1$ |
| $F_p$ | $g_{7/2}$ [404]7/2 | $(+,+1/2)_1$ |
| $X_p$ | $h_{9/2}$ [541]1/2 | $(+,-1/2)_2$ |
| $Y_p$ | $h_{9/2}$ [541]1/2 | $(+,+1/2)_2$ |

In order to check the validity of the proposed configurations, from the aligned angular momentum and the systematics of the region, the experimental $B(M1)/B(E2)$ ratios have been compared with those predicted from theoretical calculations. The intensity branching ratios from the data, $\lambda$, were used to calculate the experimental $B(M1)/B(E2)$ ratios using the standard relations

$$\frac{B(M1;I\rightarrow I-1)}{B(E2;I\rightarrow I-2)}=0.693\frac{E_\gamma^5(I\rightarrow I-2)}{E_\gamma^3(I\rightarrow I-1)}\frac{1}{\lambda(1+\delta^2)} \quad (1)$$

in units of $(\mu_N/e\ \mathrm{b})^2$.

The theoretical calculations were based on the geometric model of Dönau and Frauendorf [18]. In this model the ratio of reduced transition probabilities for the $\Delta I=1$ to $\Delta I=2$ transitions is calculated with

$$\begin{aligned}\frac{B(M1:I\rightarrow I-1)}{B(E2:I\rightarrow I-2)}=&\frac{12}{5Q_0^2\cos^2(\gamma+30^\circ)}\left[1-\frac{K^2}{1-(\frac{1}{2})^2}\right]^{-2}\\&\times\left\{\left(1-\frac{K^2}{I^2}\right)^{1/2}\left[K_1(g_1-g_R)\right.\right.\\&\times\left(1\pm\frac{\Delta e'}{\hbar\omega}\right)+\sum_n K_n(g_n-g_R)\Big]\\&\left.-\frac{K}{I}\left[(g_1-g_R)i_i+\sum_n(g_n-g_R)i_n\right]\right\}^2,\end{aligned} \quad (2)$$

where

$$K=K_1+K_2+K_3+\cdots. \quad (3)$$

TABLE IV. Parameters used in the theoretical $B(M1)/B(E2)$ ratio calculation from the geometric model; see text for details. Additionally the quadrupole moment was taken to be 5.5 $e$ b, $\gamma = 1°$, and $g_R = Z/A$.

| Neutron state | Shell | $g$ factor | alignment, $i$ | $K$ |
|---|---|---|---|---|
| A,B [660]1/2 | $i_{13/2}$ | −0.177 | 5.5 | 1/2 |
| E,F [521]3/2 | $f_{7/2}$ | −0.328 | 2.5 | 3/2 |
| X,Y [505]11/2 | $h_{11/2}$ | −0.209 | 1.0 | 11/2 |
| Proton orbit | Shell | $g$ factor | alignment, $i$ | $K$ |
| $A_p$,$B_p$ [523]7/2 | $h_{11/2}$ | +1.214 | 2.5 | 7/2 |
| $E_p$,$F_p$ [404]7/2 | $g_{7/2}$ | +0.739 | 1.0 | 7/2 |

The subscripts $n$ refer to the quasiparticles, or aligned pairs of quasiparticles, that couple to form the band. $\Delta e'$ is the signature splitting of the level energies in the rotating frame. Quasiparticle 1 is deemed to be the particle responsible for the signature splitting. In the calculation the signature-splitting term was set to zero so that just the average theoretical $B(M1)/B(E2)$ ratio was determined. In addition the $B(E2)$ value was calculated assuming a quadrupole moment of 5.5 $e$ b from a rough average of the measured values in $^{157}$Ho [19]. Table IV shows the values of the parameters that were used in the calculation.

The actual experimental signature splitting between the states of the strongly coupled bands in $^{156}$Ho, observed in these data, was estimated according to

$$\Delta E_{\text{split}} = E(I) - E(I-1) - \frac{1}{2}[E(I+1) - E(I) + E(I-1) - E(I-2)], \quad (4)$$

where $E(I)$ is the excitation energy (in keV) of the state with spin $I\hbar$.

### A. Configurations of the bands

The high-spin systematic behavior of the nuclei around $^{156}$Ho is dominated by the presence of the neutron intruder $i_{13/2}$ and proton $h_{11/2}$ orbitals. These high-$j$ orbitals lie close to the Fermi surface at zero rotational frequency and decrease rapidly in energy as the rotational frequency increases. Bands 1a and 1b have the lowest excitation energy at low spin and are expected to be built upon the lowest neutron configuration, A, $i_{13/2}$ [660]1/2$^+$ coupled with both signatures, $A_p$ and $B_p$, of the the lowest proton configuration, $h_{11/2}$ [523]7/2$^-$. Figure 3 shows the experimental aligned angular momentum, $i$, versus rotational frequency extracted from the data, using the prescription of Ref. [20], for all of the bands observed in $^{156}$Ho and the yrast band in $^{156}$Dy [21] for comparison. A reference term, representing the contribution from the collective rotation of the nucleus, has been subtracted according to Harris [22] with parameters, $\mathcal{I}_0 = 32.1$ MeV$^{-1}\hbar^2$ and $\mathcal{I}_1 = 34.0$ MeV$^{-3}\hbar^4$ from Refs. [21,23]. The $^{156}$Dy data show the back-bending effect of the first (AB) alignment ($\Delta i = 10\hbar$) of a pair of $i_{13/2}$ neutrons near $\hbar\omega \approx 0.28$ MeV. In the neighboring nuclei the AB band crossing occurs at $\hbar\omega \approx 0.27$ MeV in $^{157}$Ho [8], at $\hbar\omega \approx 0.3$ MeV in $^{155}$Ho [7,24] and at $\hbar\omega \approx 0.28$ MeV in $^{158}$Er [25].

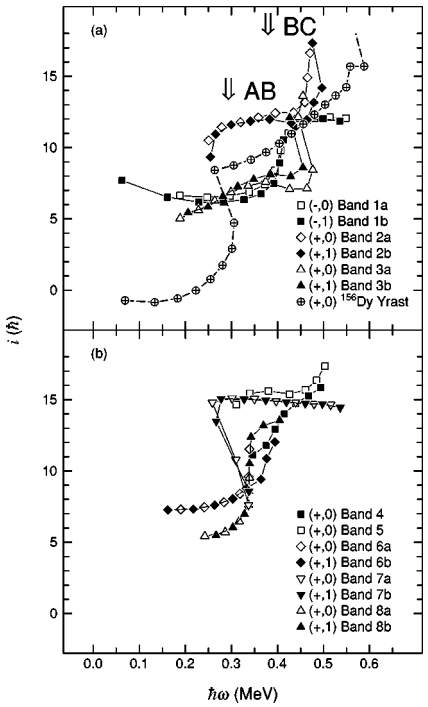


FIG. 3. (a) The experimental aligned angular momentum as a function of rotational frequency for bands 1, 2 and 3 in $^{156}$Ho and the $i_{13/2}$ band in $^{156}$Dy for comparison. (b) The experimental aligned angular momentum for bands 4, 5, 6, 7, and 8 in $^{156}$Ho. The Harris parameters $\mathcal{I}_0 = 32.1\ \hbar^2$/MeV and $\mathcal{I}_1 = 34\hbar^4$/MeV$^3$ were used as a reference band.

#### 1. Bands 1a and 1b

Figure 3(a) shows that neither signature of the $^{156}$Ho yrast bands 1a or 1b undergo the first (AB) neutron band crossing. This nonobservation of the AB crossing in $^{156}$Ho is consistent with the configurations of bands 1a and 1b involving either the A or the B orbital since the AB crossing would then be blocked. The value of the aligned angular momentum ($\approx 5\hbar$) of these bands at low frequency, $\hbar\omega \approx 0.1$–$0.2$ MeV, rules out the possibility that both A and B are occupied ($i_A + i_B = 10\hbar$). Figure 3(a) also shows that bands 1a and 1b undergo a crossing at $\hbar\omega \approx 0.40$ MeV with an aligned angular momentum gain $\Delta i = 5.0\hbar$. The behavior of this crossing is consistent with that expected for a BC crossing [26]. In this case the configuration for the yrast bands can be built upon neither the B nor the C orbitals. (In $^{157}$Ho [8] the BC crossing occurs at a rotational frequency of $\hbar\omega \approx 0.37$ MeV with an aligned angular momentum gain of $\Delta i \approx 5.9\hbar$.) Therefore, we assign the initial low-spin neutron configuration for bands 1a and 1b as the A orbit.

Employing similar blocking arguments for the proton configurations then the nonobservation of the first proton band crossing, $A_pB_p$, which takes place at $\approx 0.43$ MeV in $^{157}$Ho and the neighboring nuclei [21,23,27], can be understood if the configuration of bands 1a and 1b are built upon the lowest $A_p$ and $B_p$ $h_{11/2}$ proton [523]7/2 orbitals. In conclusion all of these observations are consistent with bands 1a

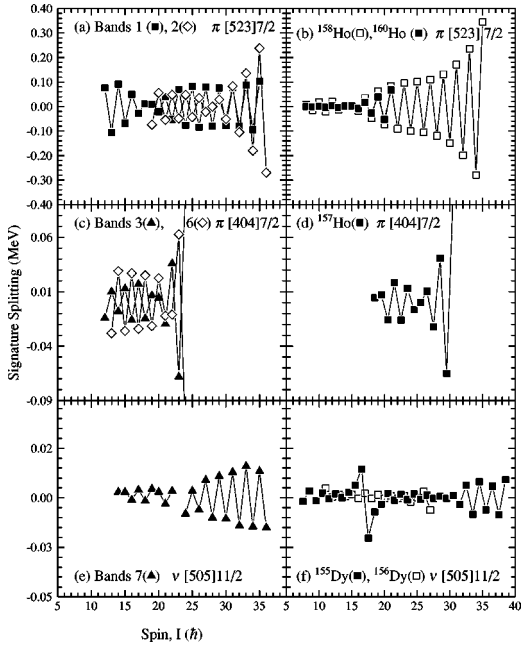


FIG. 4. Signature splitting as a function of spin (see text) for (a) bands 1 (filled squares) and 2 (open diamonds) based on the [523]5/2 orbit in $^{156}$Ho, (b) [523]7/2 bands in $^{158}$Ho (open squares) and $^{160}$Ho, (filled squares) (c) bands 3 (filled triangles) and 6 (open diamonds) $^{156}$Ho, (d) [404]7/2 bands (filled squares) in $^{157}$Ho, (e) bands 7 (filled triangles) based on [505]11/2 configuration in $^{156}$Ho, (f) bands based on [505]11/2 orbital on $^{155}$Dy (filled squares) and $^{156}$Dy (open squares). Note the ordinate scale change between the first, second and third panels.

and 1b having the $AA_p$ and $AB_p$ configurations, respectively.

The experimental signature splitting for bands 1a and 1b, which is governed by the lowest $A_p$ and $B_p$ $h_{11/2}$ [523]7/2 proton orbitals, is shown by the filled squares in Fig. 4(a). Also shown in Fig. 4(b) is the signature splitting of the corresponding bands, built upon similar configurations, in the neighboring nuclei, $^{158}$Ho (open squares) [28,29] and in $^{160}$Ho (filled squares) [30]. From Figs. 4(a) and 4(b) it can be observed that the signature splitting between bands 1a and 1b and that in the $h_{11/2}$ [523]7/2 bands in $^{158}$Ho and $^{160}$Ho are similar above spin $20\hbar$. However, one difference should be pointed out: the signature splitting at low spin in $^{156}$Ho is larger than that of $^{158}$Ho and at high spin this signature splitting is comparable. The open diamonds in Fig. 4(a) will be discussed in Sec. IV A 2.

The experimental $B(M1)/B(E2)$ ratios for bands 1a and 1b, Fig. 5(a), exhibit a regular staggering between the states of odd and even spin and have an experimental $B(M1)/B(E2)$ ratio of about $1.1\mu_N/e\ \mathrm{b}^2$ at spin (14) which reduces to about $0.5\mu_N/eb^2$ at spin $(24)\hbar$. The theoretical values (solid lines) based on the $AA_p$ proposed configurations (assuming zero signature splitting) qualitatively reproduce this trend. In summary bands 1a and 1b are well described by the proposed $AA_p$ and $AB_p$ configurations assignments. These configuration assignments and those for the other bands in $^{156}$Ho are summarized in Table V.

### *2. Bands 2a and 2b*

Figure 3(a) shows that bands 2a and 2b have a larger experimental aligned angular momentum at low rotational

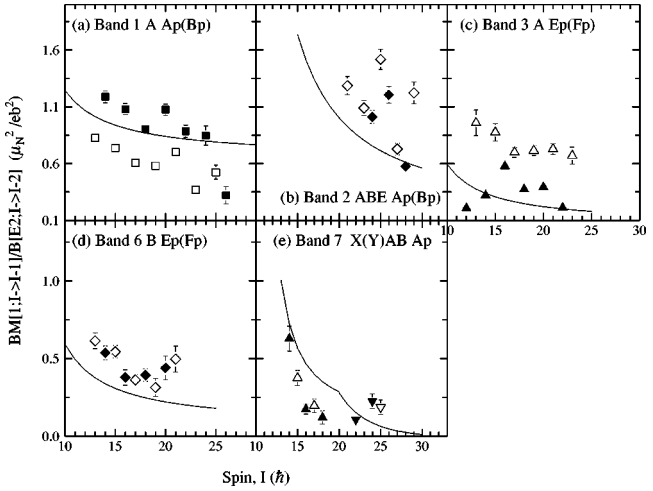


FIG. 5. Experimental and theoretical $B(M1)/B(E2)$ ratios as a function of spin for bands 1a, 1b, 2a, 2b, 3a, 3b, 6a, 6b, 7a, and 7b in $^{156}$Ho. The solid line represents the theoretical calculated from the semiclassical model of Dönau and Frauendorf based on the proposed configurations; see text for details. Filled symbols refer to signature 0 states and open symbols refer to signature 1 states. In the figure, the uncertainties result from the uncertainty in the gamma-ray intensities and do not include those which result from the choice of parameters employed in the calculation.

frequencies than that of the yrast bands 1a and 1b. We argue that this is because bands 2a and 2b are based upon a configuration involving the aligned pair of $i_{13/2}$ neutrons, AB. Notice how the curve for bands 2a and 2b seem to follow on from the $^{156}$Dy points after the back-bending point at 0.25 MeV [21]. Further, if bands 2a and 2b involve both the A and the B orbitals, then neither the BC nor the AD crossings would be expected to occur. This is consistent with the observation that no crossing takes place around $\hbar\omega \approx 0.40$ MeV [8]; see Fig. 3(a). From a study of the neighboring nuclei and the CSM predictions the next lowest neutron orbital that this band could be built upon is the negative parity E, $h_{9/2}$ [521]3/2 orbit.

TABLE V. Summary of the configuration assignments for the rotational bands observed in $^{156}$Ho.

| Band | Configuration |
|---|---|
| 1a | $AA_p \rightarrow ABCA_p$ |
| 1b | $AB_p \rightarrow ABCB_p$ |
| 2a | $EABA_p \rightarrow$ Band termination |
| 2b | $EABB_p \rightarrow$ Band termination |
| 3a | $AE_p \rightarrow$ Band termination |
| 3b | $AF_p \rightarrow$ Band termination |
| 4 | $X_pA \rightarrow X_pABC$ |
| 4 | (alternative configuration $X_pA \rightarrow X_pAA_pB_p$) |
| 5 | $X_pEAB$ |
| 6a | $BF_p$ |
| 6b | $BE_p$ |
| 7a | $XA_p \rightarrow XABA_p$ |
| 7b | $YA_p \rightarrow YABA_p$ |
| 8a | $XA_p \rightarrow XBCA_p$ |
| 8b | $YA_p \rightarrow YBCA_p$ |

The second gain in aligned angular momentum which occurs in this band at $\hbar\omega \approx 0.45$ MeV in Fig. 3(a) cannot be fully reconciled with that expected from the first pair of protons $A_pB_p$. This is because, in this region, this alignment usually occurs over a large range in rotational frequency as a consequence of its large interaction strength [21,23,27] as illustrated by the $^{156}$Dy yrast band in Fig. 3(a) from $\hbar\omega \approx 0.35-0.55$ MeV. In addition, Fig. 3(a) also shows that the gain in aligned angular momentum, $\Delta i \approx 5-6\hbar$, continues to rise even at the highest observed rotational frequencies. The nature of this anomalous aligned angular momentum gain will be discussed in the Sec. IV B. In summary, bands 2a and 2b are interpreted as being built upon a configuration which has the EAB orbitals coupled to the proton $A_p$ and $B_p$ orbitals. These bands are, therefore, based upon the $ABEA_p$ and $ABEB_p$ configurations.

The signature splitting in bands 2a and 2b is governed by that of the proton $h_{11/2}$ [523]7/2 orbital which is expected to be similar in magnitude to that shown by bands 1a and 1b. Figure 4(a) shows this similarity and Fig. 4(b) the similarity with bands based on the $\pi$ [523]7/2 orbital in the neighboring nuclei $^{158}$Ho and $^{160}$Ho. Interestingly, signature inversion occurs in both bands 1a and 1b and bands 2a and 2b but at a different spin. The theoretical $B(M1)/B(E2)$ ratios for bands 2a and 2b based on the $EBAA_p$ configuration are also in qualitative agreement with these data; see Fig. 5(b). From this comparison with the neighboring nuclei and bands 1a and 1b it can be deduced that there is good agreement with the proposed configuration for bands 2a and 2b.

#### *3. Bands 3a and 3b*

Bands 3a and 3b do not show any evidence for an AB neutron band crossing around $\hbar\omega \approx 0.25-0.30$ MeV; see Fig. 3(a). This implies that the AB configuration is blocked for these bands and that they are built upon either the A or the B orbital. The possibility for both A and B being occupied is ruled out since the low frequency aligned angular momentum is small ($\approx 5\hbar$). It can also be observed that bands 3a and 3b appear to undergo a smooth increase in aligned angular momentum from 0.25 to 0.4 MeV; see Fig. 3(a). This increase could be associated with the BC crossing which would imply that bands 3a and 3b are built upon the neutron A $i_{13/2}$ [660]1/2 configuration. Alternatively this increase could arise from the AD crossing which would imply that bands 3a and 3b are built upon the neutron B $i_{13/2}$ [660]1/2 configuration. However, in this mass region the $A_pB_p$ proton crossing also takes place around these rotational frequencies [see the smooth aligned angular momentum increase in the $^{156}$Dy yrast band in Fig. 3(a)] which is similar to the behavior of bands 3a and 3b over the rotational frequency range (0.25 to 0.4 MeV). Furthermore, the nonobservation of this interaction in bands 1a and 1b and bands 2a and 2b is consistent because both of their configuration assignments contain either the $A_p$ or $B_p$ quasiparticle. These aligned angular momentum properties are consistent with the bands having $E_p$ and $F_p$ proton $g_{7/2}$ [404]7/2 configurations.

Another gain in aligned angular momentum occurs at 0.45 MeV for bands 3a and 3b; see Fig. 3(a). This gain is at least $\approx 5-6\hbar$ and continues to rise even at the highest observed rotational frequencies. This alignment gain is similar to that observed in bands 2 and will be discussed in Sec. IV B.

Figure 4(c) shows the signature splitting for bands 3a and 3b; notice the scale change between Figs. 4(a) and 4(c). Also shown in the figure is the signature splitting observed in a band based upon a similar proton $g_{7/2}$ [404]7/2 configuration in the neighboring nucleus $^{157}$Ho [8], Fig. 4(d). Reasonable agreement in these nuclei with the absolute magnitude of the splitting is observed. The experimental $B(M1)/B(E2)$ ratios for bands 3a and 3b have an average ratio of about $0.5\mu_N/e\ \mathrm{b}^2$ for all spins. The theoretical ratios based on the $AE_p(F_p)$ configuration qualitatively reproduce this trend as a function of spin; see Fig. 5(c). In summary band 3a is interpreted as being built upon the $AE_p$ and band 3b upon the $AF_p$ configuration.

#### *4. Band 4*

The configuration assignment for band 4 has been deduced from its aligned angular momentum shown in Fig. 3(b) and the fact that it is a decoupled band which means it must be based upon an orbit which has large signature splitting. The lowest-lying proton orbital with a large signature splitting, from the systematics of the neighboring nuclei, is the $X_p$ $h_{9/2}$ [541]1/2 orbit. A decoupled band with similar alignment properties has been observed in $^{157}$Ho [8]. Since band 4 shows no evidence for the AB band crossing, its configuration must, therefore, be built upon either the A or the B orbital. However, at a rotational frequency of $\hbar\omega \approx 0.43$ MeV a smooth increase in aligned angular momentum is observed; see Fig. 3(b). This aligned angular momentum gain is most probably caused by the alignment of a pair of BC neutrons. Comparison with the BC crossing observed in the yrast bands 1a and 1b reveals that the total aligned angular momentum gain, $5\hbar$, is very similar. Therefore, band 4 is assigned an $AX_p$ configuration at low rotational frequencies and an $ABCX_p$ configuration at higher rotational frequencies. However, there are alternative configuration assignments which could also explain the behavior of band 4. For example, the $X_p$ $h_{9/2}$ [541]1/2 orbit could increase the deformation which may in turn reduce the frequency at which the BC crossing takes place. In this case the crossing observed at $\hbar\omega \approx 0.43$ MeV could be the $A_pB_p$ crossing and band 4 might be based on the $AX_pA_pB_p$ configuration.

#### *5. Band 5*

Band 5 is also a decoupled band and exhibits very similar behavior to the bands 2a and 2b above the AB band crossing in that its initial aligned angular momentum at its lowest observed rotational frequency is large. Indeed, Fig. 3(b) indicates that band 5 shows the start of a decrease in aligned angular momentum at low rotational frequencies where the AB band crossing is expected and therefore, can neither be built upon the A nor the B orbital below this rotational frequency. The next lowest neutron orbit is the E, $f_{7/2}$ [521]3/2 orbital. At frequencies around $\hbar\omega = 0.46$ MeV band 5 gains aligned angular momentum which is interpreted as the start of the proton $A_pB_p$ band crossing. In this case band 5 cannot be built upon either the $A_p$ or $B_p$ configuration and must be built upon a proton configuration which has a large signature splitting since it is a decoupled band. The systematics of the neighboring nuclei suggest that this is most likely the proton

$h_{11/2}$ [541]1/2 $X_p$ orbital. Therefore, band 5 is assigned a four-quasiparticle $E(AB)X_p$ configuration above the AB band crossing. A band with similar properties has been observed in $^{157}$Ho [8].

#### *6. Bands 6a and 6b*

Bands 6a and 6b do not show any evidence for the AB band crossing; see Fig. 3(b), which implies that the configuration of these bands involve either the A or B orbits being occupied. Since the low frequency aligned angular momentum is about $7\hbar$, bands 6a and 6b cannot have both A and B occupied. Figure 3(b) shows that a gain in aligned angular momentum occurs around 0.35 MeV which is consistent with the BC crossing. In this case bands 6a and 6b would be built upon the A orbital coupled with one of the lower proton orbitals, for example, the $AE_p$ and $AF_p$ configurations. However, since the more intensely populated bands 3a and 3b are already associated with the $AE_p$ and $AF_p$ configurations, the crossing at 0.35 MeV, in bands 6a and 6b, is more likely the AD crossing. In this case the configurations for bands 6a and 6b could be based on the $BE_p$ and $BF_p$ orbits and would be less intensely populated than bands 3a and 3b, which is consistent with these data; see Table I. Unfortunately bands 6a and 6b were not observed to sufficiently high rotational frequencies ($\geqslant$0.45 MeV) to determine whether the first proton band crossing occurs.

The signature splitting between bands 6a and 6b is shown in Fig. 4(c) and is very similar in magnitude to that of bands 3a and 3b and to that of the bands based upon similar configurations in the neighboring nuclei $^{157}$Ho [8]. The experimental $B(M1)/B(E2)$ ratios for bands 6a and 6b are about $0.5\mu_N/e$ b$^2$ for the entire spin range over which they are observed. The theoretical ratios (solid lines) based on the $BE_p$ configuration are in good agreement with the experimental ratios extracted from these data; see Fig. 5(d).

#### *7. Bands 7a, 7b and 8a, 8b*

At low rotational frequencies the signature splitting between bands 7a and 7b is very small. This suggests that these strongly coupled bands are most likely built upon configurations which have large $\Omega$ quantum numbers such as the neutron X and Y $h_{11/2}$ [505]11/2 orbital coupled with the lowest proton orbit, $A_p$. Bands with similar properties have been established in the neighboring holmium isotopes, for example, in $^{157}$Ho [8] and in $^{155}$Ho [9]. At a rotational frequency of $\hbar\omega\approx$0.3 MeV bands 7a and 7b undergo a backbend; see Fig. 3(b). This band crossing in interpreted as an AB crossing since the observed $10\hbar$ gain in alignment is only consistent with this crossing. Notice how the curves for bands 7a and 7b resemble the AB crossing observed in the $^{156}$Dy yrast band; see Fig. 3(a) and also the behavior of bands 2a and 2b above $\hbar\omega\approx$0.25 MeV. Above this rotational frequency ($\hbar\omega$=0.3 MeV) bands 7a and 7b do not show evidence for any other neutron or proton band crossings, presumably because their underlying single-particle orbit configuration blocks all possible band crossings; see Fig. 3(b). At these high rotational frequencies bands 7a and 7b are interpreted as being based on $XABA_p$ and $YABA_p$ configurations.

At rotational frequencies around $\hbar\omega\approx$0.3 two new sequences, bands 8a and 8b, are observed to feed into bands 7a and 7b; see Fig. 1(a). These bands are interpreted as the continuation of bands 7a and 7b above the AB crossing and are based on the $XA_p$ and $YA_p$ configurations. These bands undergo an alignment gain at $\hbar\omega$=0.33 MeV which is interpreted as a BC crossing.

The signature splitting between bands 7a and 7b below the AB crossing is extremely small; see Fig. 4(e). This splitting is in good agreement with that of the bands involving the [505]11/2 orbit configuration in the neighboring nuclei $^{156}$Dy [21] and $^{155}$Dy [9] and is smaller than that observed in bands 1a and 1b ([523]7/2) and bands 3a and 3b ([404]7/2) since they are based upon the signature splitting of the strongly-coupled [505]11/2 orbit. Below the AB crossing bands 7a and 7b have $B(M1)/B(E2)$ ratios of about 0.6 $\mu_N/e$ b$^2$ at spin $(14)\hbar$ which decreases to $0.1\mu_N/e$ b$^2$ at spin $(18)\hbar$. This trend is reasonably reproduced in the theoretical calculations based on the $XA_p$ configuration; see Fig. 5(e).

Above the AB crossing the experimental signature splitting between bands 7a and 7b; see Fig. 4(e), are in good agreement with those of the bands based upon similar configurations in the neighboring $^{156}$Dy [21] and $^{155}$Dy [9], Fig. 4(f). These signature splittings are smaller than those observed in bands 1a and 1b and bands 3a and 3b since they are based upon the signature splitting of the strongly coupled $h_{11/2}$ [505]11/2 orbit. The experimental $B(M1)/B(E2)$ ratios for bands 7a and 7b, above the AB crossing, have large uncertainties due to the low intensity and contamination of these bands. The theoretical ratios based on the $XABA_p$ configuration are also presented in Fig. 5(f) for comparison.

### B. Band termination

The excitation energies of the states in $^{156}$Ho are plotted in Fig. 6 versus spin relative to a rigid-rotor reference. In the figure it can be observed that the highest-spin states in bands 2a and 2b and 3a and 3b begin to show the start of a down-sloping trend compared with the excitation energy minus rigid-rotor energy above spin $30\hbar$. This trend has also been observed in the neighboring nuclei and was suggested to be characteristic of a nucleus which is undergoing a transition from collective to single-particle behavior with a corresponding nuclear shape change from weakly deformed prolate to a weakly deformed oblate [31]. When a nucleus in this mass region approaches band termination its angular momentum or spin is gained rather efficiently only requiring a relatively small amount of energy. Therefore, if the excitation energy of a rigid rotor reference is subtracted, the levels associated with the band terminating sequence should be down-sloping with respect to spin [31].

The band termination scenario was first suggested for the rotational bands in $^{155}$Ho and $^{156}$Ho in Ref. [7]. The spins at which these bands terminate is determined by the number of valence particles outside the $^{146}_{64}$Gd closed shell. For example, the dashed lines in Fig. 6 represent two of the rotational bands in $^{155}_{66}$Dy which show behavior consistent with the approach to band termination [9,32]. The theoretical calculations for this nucleus predict that there should be a low-lying $\pi[(h_{11/2})^2]\nu[(i_{13/2})^2(f_{7/2})^3(h_{9/2})^2]$ configuration which terminates at spin $75/2^-$ $\hbar$ [32]. In agreement with this scenario, Emling *et al.* [32] presented evidence that the

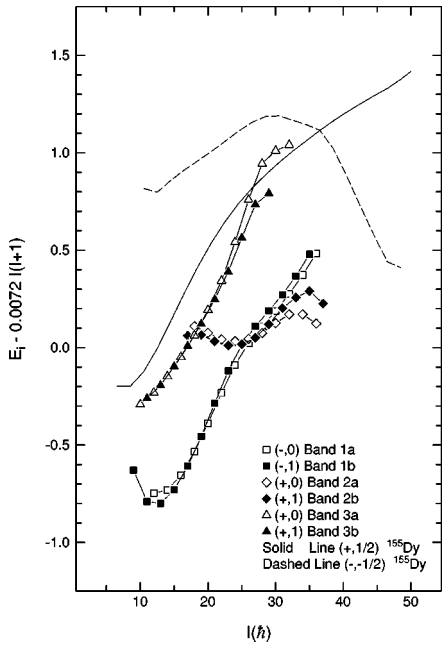


FIG. 6. Excitation energy of the states in bands 1, 2, and 3 relative to a rigid rotor. The EAB configuration which terminates in $^{155}$Dy is shown with a dashed line for comparison. The solid line represents the ABC configuration in $^{155}$Dy which shows no evidence for band termination.

high-spin states in this band at spins $71/2^-$ and $75/2^-$ were long-lived with lifetimes greater than 1.5 ps.

In an analogous manner two terminating states with especially low excitation energies have been observed in $^{157}$Ho [8] at spins $75/2^-$ and $87/2^-\hbar$. The $87/2^-$ state was described as a closed $^{146}$Gd core with eleven valence particles in a fully aligned

$$\pi[(h_{11/2})^3]_{(27^-/2)}\otimes\nu[(i_{13/2})^2(f_{7/2})^3(h_{9/2})^3]_{30+}$$

configuration. The $75/2^-$ state has one $f_{7/2}$ neutron antialigned with a

$$\pi[(h_{11/2})^3]_{(27^-/2)}\otimes\nu[(i_{13/2})^2(f_{7/2})^4_{4+}(h_{9/2})^2]_{24+}$$

configuration. In $^{157}$Ho the lifetime measurements described in Ref. [19] were consistent with the interpretation of band termination because the high-spin states ($>72/2$) were observed to be long lived with lifetimes greater than 1.1 ps. Indeed an 8 ps lifetime was deduced for the $75/2^-$ state, corresponding to a transition quadrupole moment of $\leqslant 1\ e$ b which is consistent with the extremely weak collectivity expected for these band terminating states. The heavier Er nuclei show similar behavior, for example, in $^{157}$Er [23] and $^{158}$Er [33], many single-particle and fully aligned band terminating states are observed at spins around $40^+$ and $46^+\hbar$.

Thus in $^{156}$Ho, which has 10 valence particles, low-lying $\pi(h_{11/2})^3\otimes\nu[(i_{13/2})^2(f_{7/2})^3(h_{9/2})^2]$ configurations which terminate at spins $40^+$ and $41^+$ are expected. In $^{155}_{66}$Dy [9] it was observed that the bands based upon the EAB and FAB configurations showed a decrease in excitation energy minus rigid-rotor value above spins $\approx 30\hbar$ where they are crossed by the terminating sequences; see the dashed lines in Fig. 6. In $^{156}_{67}$Ho an analogous situation seems to occur when the $\mathrm{EABA}_p(\mathrm{B}_p)$ configuration of bands 2a and 2b start to downslope near spin $35\ \hbar$ where they are presumably crossed by the $\pi(h_{11/2})^3\otimes\nu[(i_{13/2})^2(f_{7/2})^3(h_{9/2})^2]$ configuration; see Fig. 6. If these down-sloping terminating sequences cut through the yrast line in this manner, then based on an extrapolation of the $^{155}$Dy data, it is expected that the higher-lying nonyrast (+,0), (+,1) bands are crossed at slightly lower spins; see Fig. 6. Such a scenario is consistent with the anomalous alignment behavior of bands 3a and 3b at high spin. Note also that the configurations involving the ABC (bands 1a and 1b) and ABX(Y) (bands 8a and 8b) orbitals in $^{156}$Ho do not show any evidence for downsloping at the highest spins consistent with the behavior of bands based on similar configurations in $^{155}$Dy; see the solid lines in Fig. 6.

Therefore, it appears that the most likely explanation for this anomalous gain in aligned angular momentum in bands 2a and 2b and 3a and 3b in $^{156}$Ho is due to the fact that they are starting to undergo a change from collective to a single-particle nature with a corresponding change in shape which affects the aligned angular momentum. However, with the statistics of the present data it was not possible to observe these bands up to sufficiently high spin to observe the actual band terminating or favored high-spin states in $^{156}$Ho. Interestingly the observation of these favored states, at their specific angular momentum values, could be used to make strong arguments for the low-spin assignments of the states in this nucleus. Indeed, further data are required to probe the bands in $^{156}$Ho at higher spin and ultimately lifetime information on the higher-spin states should confirm the weak collectivity of these states and the existence of band termination.

## V. SUMMARY

In summary new rotational bands have been established and the previous level scheme considerable extended in $^{156}$Ho with the Gammasphere spectrometer. Configurations for these bands have been deduced from their aligned angular momenta, signature splittings and from a systematic survey of the neighboring nuclei and these are compared with theoretical $B(M1)/B(E2)$ predictions from a semiclassical model. Good agreement is found with the proposed configurations. Evidence is presented for the approach to band termination, at the highest spin states in two of these strongly coupled bands which is consistent with the expectations from neighboring nuclei where this phenomenon has been established. However, detailed lifetime measurements are ultimately required to measure the reduction in the collectivity of these states.

## ACKNOWLEDGMENTS

The authors would like to thank P. Fallon, I. Y. Lee, A. O. Macchiavelli, R. W. MacLeod and the crew of the 88-Inch Cyclotron for their assistance during the experiment and H. Jin for supplying the ''Jinware'' software. J. Simpson and M. A. Riley acknowledge receipt of a NATO Collaborative Research Grant. The Nuclear Structure Research Laboratory at Rochester is supported by the NSF under Contract No. PHY-9220318 and Florida State University acknowledges support from the NSF and the State of Florida.

[1] R. Neugart, E. Arnold, W. Borchers, W. Neu, G. Ulm, and K. Wendt, in *Proceedings of the 5th International Conference on Nuclei Far from Stability*, Rosseau Lake, Canada 1987, edited by I. S. Towner (American Institute of Physics, New York, 1988), p. 126.
[2] G. D. Alkhazov, A. E. Barzakh, I. Ya. Chubukov, V. P. Denisov, V. S. Ivanov, N. B. Buyanov, V. N. Fedoseyev, V. S. Letokhov, V. I. Mishin, and S. K. Sekatsky, Nucl. Phys. **A504**, 549 (1989).
[3] K. D. Schilling, L. Kaubler, W. Andrejtscheff, T. M. Muminov, V. G. Kalinnikov, N. Z. Marupov, F. R. May, and W. Seidel, Nucl. Phys. **A299**, 189 (1978).
[4] R. G. Helmer, Nucl. Data Sheets **65**, 65 (1992); **49**, 383 (1986).
[5] R. Bengtsson *et al.*, Nucl. Phys. **A415**, 189 (1984).
[6] T. Bentgsson and I. Ragnarsson, Phys. Scr. **T5**, 165 (1983).
[7] J. Simpson *et al.*, Proceedings of XXIII International Winter Meeting on Nuclear Physics, Bormio, Italy, 1985; R. V. F. Janssens (private communication).
[8] D. C. Radaford *et al.*, Nucl. Phys. **A545**, 665 (1992).
[9] R. Vlastou *et al.*, Nucl. Phys. **A580**, 133 (1994).
[10] S. J. Gale *et al.*, J. Phys. G **21**, 193 (1995).
[11] I. Y. Lee, Nucl. Phys. **A520**, 641c (1990).
[12] D. C. Radford, Nucl. Instrum. Methods Phys. Res. A **361**, 297 (1995).
[13] K. S. Krane, R. M. Steffen, and R. M. Wheeler, Nucl. Data Tables **11**, 351 (1973).
[14] J. Waddington *et al.*, Scientific/Technical Report No. 147, University of Bergen, Norway, 1984.
[15] S. H. Bhatti *et al.*, Z. Phys. A **353**, 119 (1995).
[16] G. Løvhøiden, Phys. Scr. **25**, 459 (1982).
[17] W. Nazarewicz, R. Wyss, and A. Johnson, Nucl. Phys. **A503**, 285 (1989).
[18] F. Dönau and S. Frauendorf, in *Proceedings of the Conference on High Angular Momentum Properties of Nuclei*, Oak Ridge, Tennessee, 1982, edited by N. R. Johnson (Harvard Academic, New York, 1983); F. Dönau, Nucl. Phys. **A471**, 469 (1987).
[19] H. Gascon *et al.*, Nucl. Phys. **A513**, 344 (1990).
[20] R. Bengtsson and S. Frauendorf, Nucl. Phys. **A314**, 27 (1979); **A327**, 139 (1979).
[21] M. A. Riley *et al.*, Nucl. Phys. **A486**, 456 (1988).
[22] S. Harris, Phys. Rev. B **138**, 509 (1965).
[23] J. Simpson *et al.*, J. Phys. G **12**, L67 (1986).
[24] G. B. Hagemann, B. Herskind, J. Kownacki, B. M. Nyako, P. J. Nolan, J. F. Sharpey-Schafer, and P. O. Tjom, Nucl. Phys. **A424**, 365 (1984).
[25] J. Simpson, P. A. Butler, P. D. Forsyth, J. F. Sharpey-Schafer, J. D. Garrett, G. B. Hagemann, B. Herskind, and L. P. Ekström, J. Phys. G **10**, 383 (1984).
[26] J. D. Morrison, J. Simpson, M. A. Riley, H. W. Cranmer-Gordon, P. D. Forsyth, D. Howe, and J. F. Sharpey-Schafer, J. Phys. G **15**, 1871 (1989).
[27] M. A. Riley, J. Simpson, M. A. Bentley, P. Fallon, P. D. Forsyth, J. C. Lisle, J. D. Morrison, E. S. Paul, J. F. Sharpey-Schafer, and P. M. Walker, Z. Phys. A **345**, 121 (1993).
[28] N. Rizk and J. Boutet, J. Phys. (France) Lett. **37**, L197 (1976).
[29] C.-H. Yu, D. M. Cullen, D. Cline, M. Simon, D. C. Radford, I. Y. Lee, A. O. Macchiavelli, in *Proceedings of the workshop on Gammasphere Physics*, Berkeley, California, 1995, edited by M. A. Deleplanque, I. Y. Lee, and A. O. Macchiavelli (World Scientific, Singapore, 1996), p. 254.
[30] J. A. Pinston, S. Andre, D. Barneoud, C. Foin, J. Genevey, and H. Frisk, Phys. Lett. **137B**, 47 (1984).
[31] I. Ragnarsson, Z. Xing, T. Bengtsson, and M. A. Riley, Phys. Scr. **34**, 651 (1986).
[32] H. Emling *et al.*, Phys. Lett. B **217**, 33 (1989).
[33] J. Simpson *et al.*, Phys. Lett. B **327**, 187 (1994).